Supporting Information

Construction of efficient hole migration pathway on hematite for efficient photoelectrochemical water oxidation

*Feng Li, Jing Li, Lili Gao, Yiping Hu, Xuefeng Long, Shenqi Wei, Chenglong Wang, Jun Jin * and Jiantai Ma **

1. The equations

The conversion between potentials versus Ag/AgCl and versus RHE is determined using the equation below[1].

$$E(\text{versus RHE}) = E(\text{versus Ag/AgCl}) + E_{\text{Ag/AgCl}}(\text{refer}) + 0.0591\text{V} \times \text{pH}$$

$$E_{\text{Ag/AgCl}}(\text{refer}) = 0.197 \text{ V versus NHE at } 25\ ^{\circ}\text{C} \qquad (1)$$

Incident photon to current efficiency (IPCE) was obtained using an Oriel Cornerstone 260 1/4 m monochromator with a 500W Oriel Xe lamp as the simulated light source (LSH-X500B). An applied potential of 1.23 V vs. RHE was supplied by a miniature integrated electrochemical workstation (Zolix Instruments Co., Ltd). IPCE values were calculated using the equation below

$$IPCE(\%) = \frac{J \times 1240}{\lambda \times P_{light}} \times 100\% \qquad (2)$$

J refers to the photocurrent density (mA cm^{-2}) obtained from the electrochemical workstation. λ and P_{light} are the incident light wavelength (nm) and the power density obtained at a specific wavelength (mW cm^{-2}), respectively.

Applied bias photon-to-current efficiency (ABPE) can be calculated using the following equation:

$$ABPE(\%) = \frac{J \times (1.23 - V_b)}{P_{light}} \times 100\% \qquad (3)$$

J refers to the photocurrent density (mA cm^{-2}) obtained from the electrochemical workstation. V_b is the applied bias vs. RHE (V), and P_{light} is the total light intensity of AM 1.5 G (100 mW cm^{-2}).

The light absorption efficiency or light harvesting efficiencies (LHE, defined as the ratio of absorbed light to the incident light) of each photoanodes are calculated from their UV−Vis absorption spectra:

$$LHE = 1 - 10^{-A(\lambda)} \qquad (4)$$

where $A(\lambda)$ is the absorbance at a specific wavelength. In order to calculate J_{abs} (the photocurrent density achievable assuming 100% absorbed photon–to–current conversion efficiency for photons) the solar spectral irradiance at AM 1.5G ($W \cdot m^{-2} \cdot nm^{-1}$, ASTM G173−03) is first converted to solar photocurrents vs. wavelength ($A \cdot m^{-2} \cdot nm^{-1}$) assuming 100% IPCE for photons. Then the solar photocurrents are multiplied by the LHE at each wavelength and adding these products up.

According to the M-S curves, charge carrier density (N_d) can be calculated using the following equation[2]:

$$N_d = \frac{2}{e\varepsilon_0\varepsilon} \times \left[\frac{d\left[\frac{1}{C^2}\right]}{dV_S} \right]^{-1} \qquad (5)$$

The electronic charge (e) is 1.6×10^{-19} C, vacuum permittivity (ε_0) is 8.854×10^{-14} F m^{-1}, and relative permittivity (ε) is 80 for hematite [3]. C (F cm^{-2}) is the space charge

capacitance in the semiconductor (obtained from M-S curves), and V_s (V) is the applied potential for M-S curves.

the efficiency of charge transport in the bulk (η_{bulk}, relating to bulk charge separation) and surface charge transfer efficiency ($\eta_{surface}$, the yield of holes that are involved in water oxidation reaction after reaching the electrode/electrolyte interfaces) of the prepared photoanodes, can be calculated using the following equations:

$$\eta_{bulk} = \frac{J^{Na_2SO_3}}{J_{abs}} \quad (6)$$

$$\eta_{surface} = \frac{J^{H_2O}}{J^{Na_2SO_3}} \quad (7)$$

J_{abs} is the unity converted photocurrent density from the light absorption, while J^{H2O} and J^{Na2SO3} are the photocurrent densities obtained in 1 M KOH electrolyte and 1 M Na_2SO_3 (pH 9.5), respectively.

The electrochemically active surface area (ECSA) was estimated from the electrochemical double-layer capacitance according to a previous published report[4]. Cyclic voltammograms were performed in 1 M KOH (pH = 13.6) at the scan rate of 20, 40, 60, 80, 100, 120, 140, 160, 180 and 200 mV s^{-1} (Figure S7). Then the electrochemical active surface area was determined by measuring the capacitive current associated with double-layer charging from the scan-rate dependence of CVs. The double layer capacitance (C_{dl}) was estimated by plotting the $\triangle J = (J_a - J_c)$ at 1.05 V vs. RHE against the scan rate as shown in Figure 4a. The linear slope is equivalent to twice of the C_{dl}, which can be used to represent the electrochemical active surface area.

2. Figures

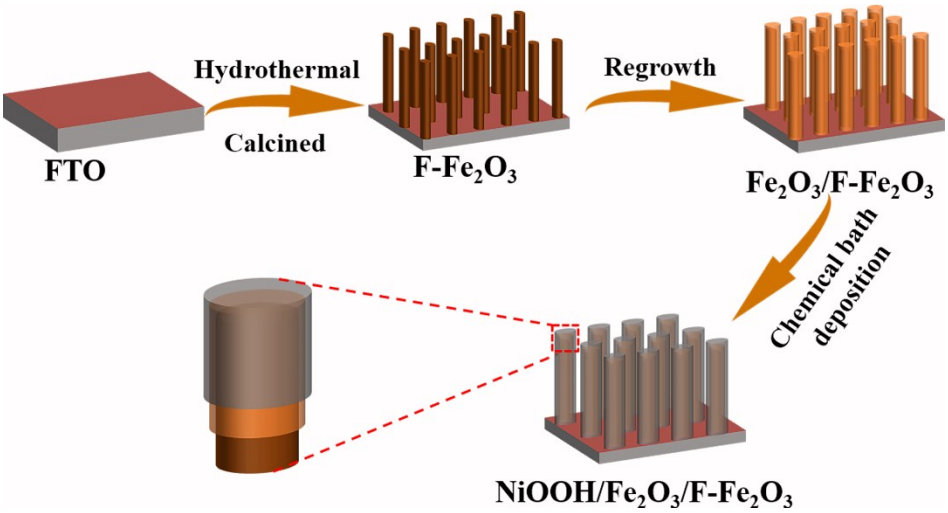

Scheme S1. Schematic diagram of the preparation procedure of the NiOOH-Fe_2O_3/F-Fe_2O_3 NRs photoanode

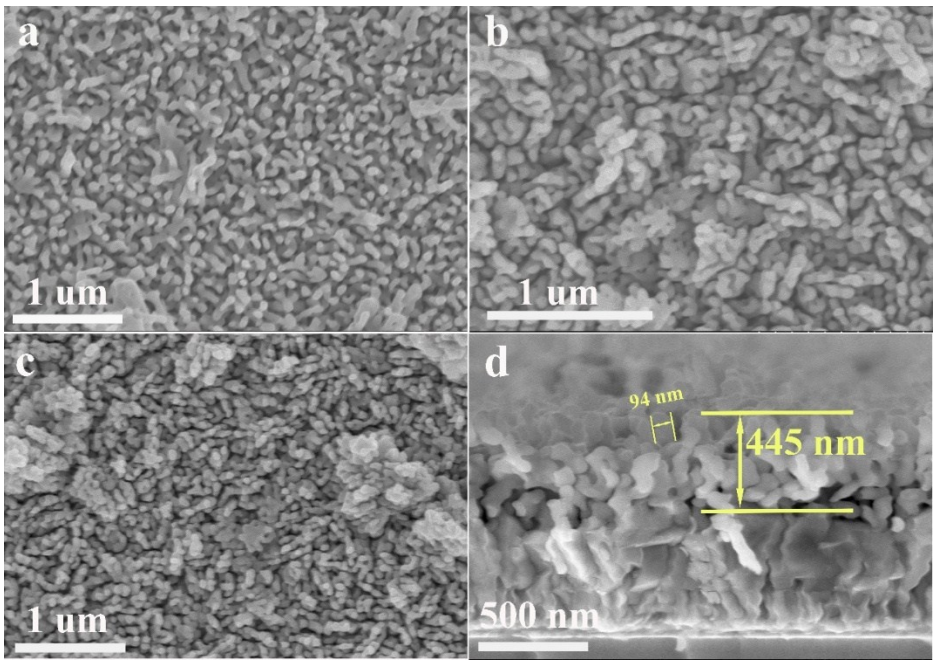

Figure S1. Top-view SEM images of (a) F-Fe_2O_3, (b) Fe_2O_3/F-Fe_2O_3, (c) NiOOH-Fe_2O_3/F-Fe_2O_3 NRs and (d) cross-section SEM image of NiOOH-Fe_2O_3/F-Fe_2O_3 NRs.

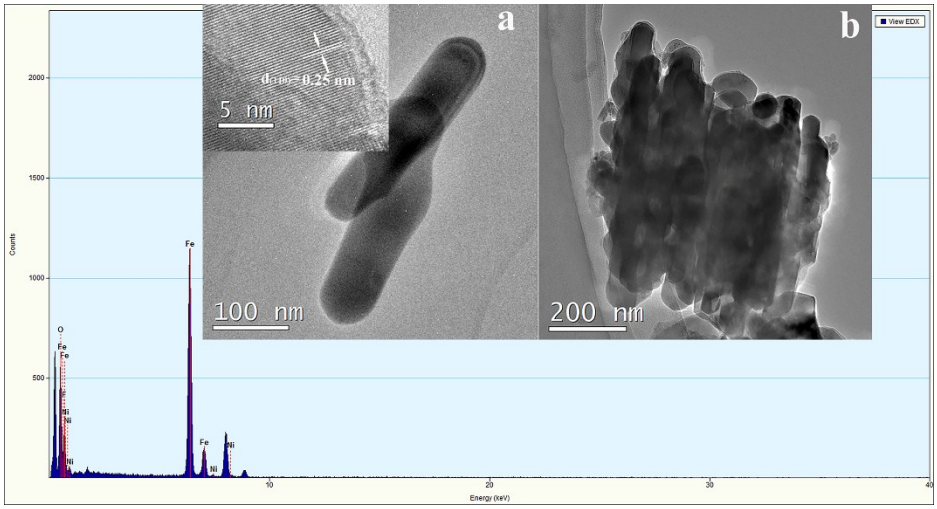

Figure S2. EDS data for NiOOH-Fe_2O_3/F-Fe_2O_3 NRs and TEM images of (a) α-Fe_2O_3 NRs, (b) NiOOH-Fe_2O_3/F-Fe_2O_3 NRs

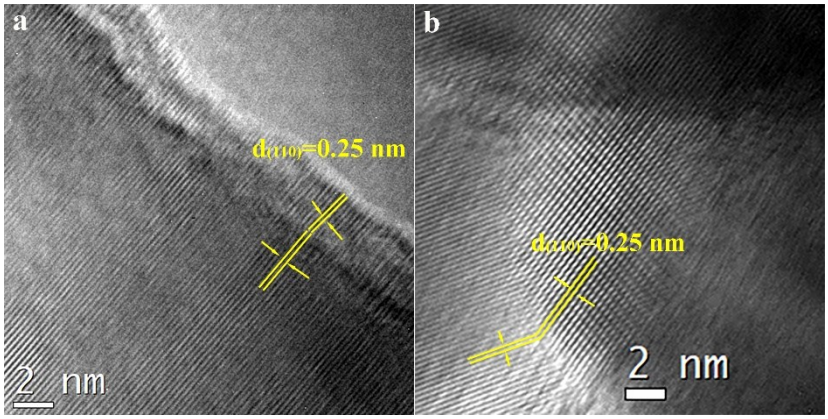

Figure S3. HRTEM image of Fe_2O_3/F-Fe_2O_3.

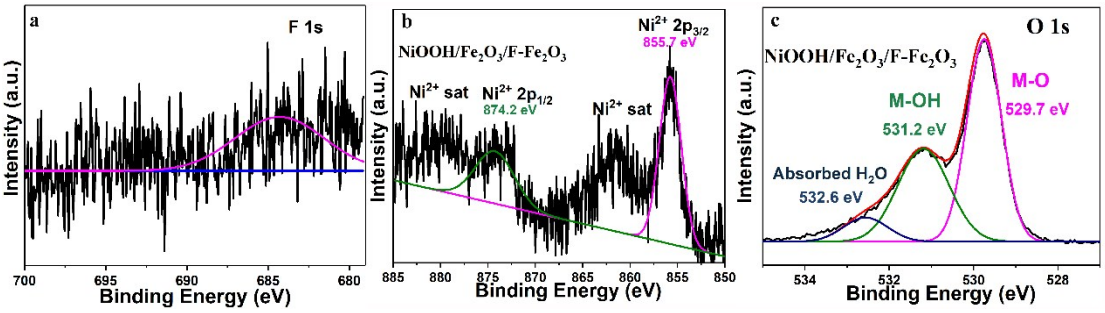

Figure S4. XPS high resolution spectrum of (a) F 1s for F-Fe_2O_3 NRs and (b) Ni 2p, (c) O 1s of NiOOH-Fe_2O_3/F-Fe_2O_3 NRs photoanode.

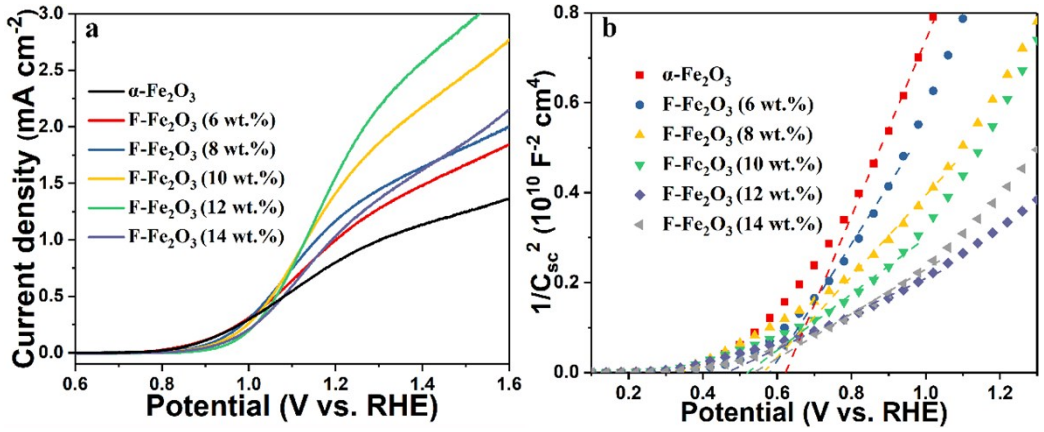

Figure S5. (a) LSVs and (b) Mott–Schottky plots of F-Fe_2O_3 with different content of F precursor collected at a fixed frequency of 1 kHz.

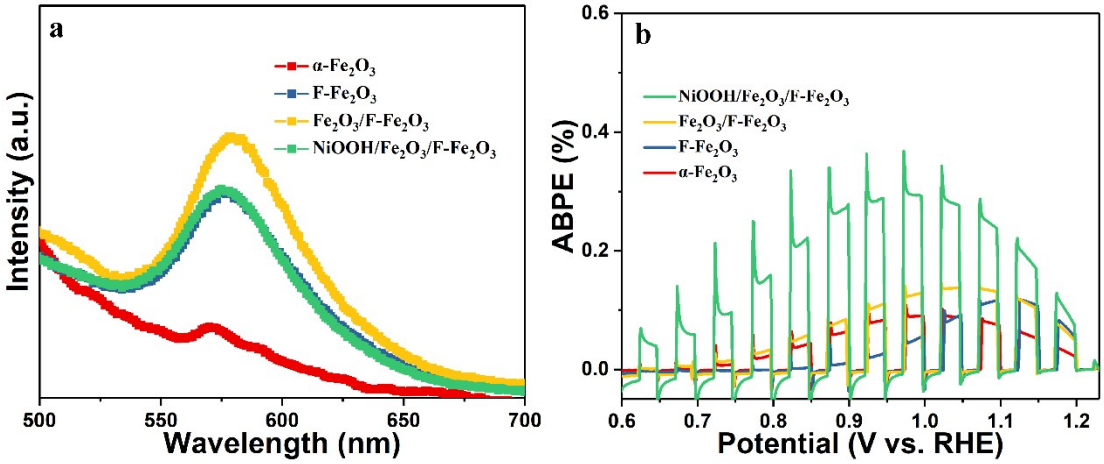

Figure S6. (a) Photoluminescence (PL) spectra and (b) ABPE of each photoanodes.

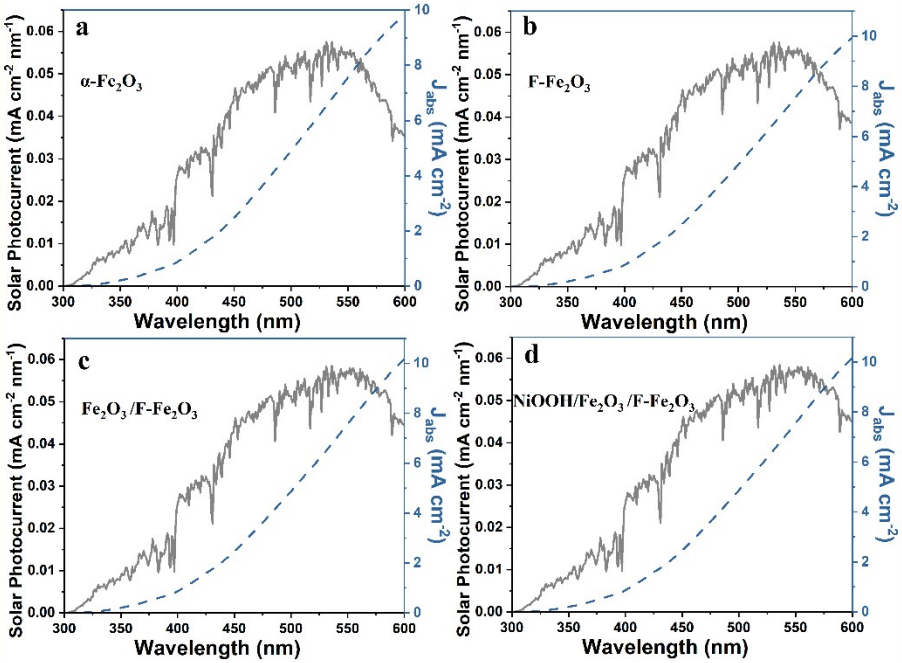

Figure S7. Jabs values of (a) α-Fe_2O_3, (b) F-Fe_2O_3, (c) Fe_2O_3/F-Fe_2O_3, and (d) NiOOH-Fe_2O_3/F-Fe_2O_3 NRs photoanodes (assuming 100% absorbed photon-to-current conversion efficiency for photons).

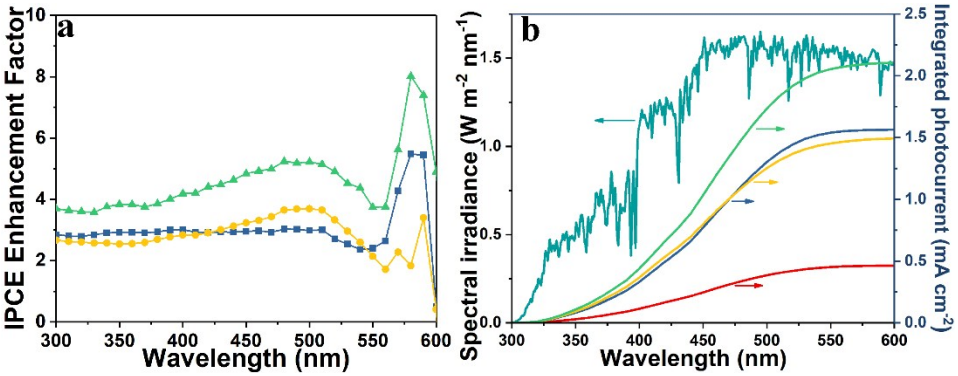

Figure S8. (a) the IPCE enhancement factors and (b) Integrated photocurrent at 1.23 V_{RHE} for α-Fe_2O_3, F-Fe_2O_3, Fe_2O_3/F-Fe_2O_3 and NiOOH/Fe_2O_3/F-Fe_2O_3 NRs photoanode.

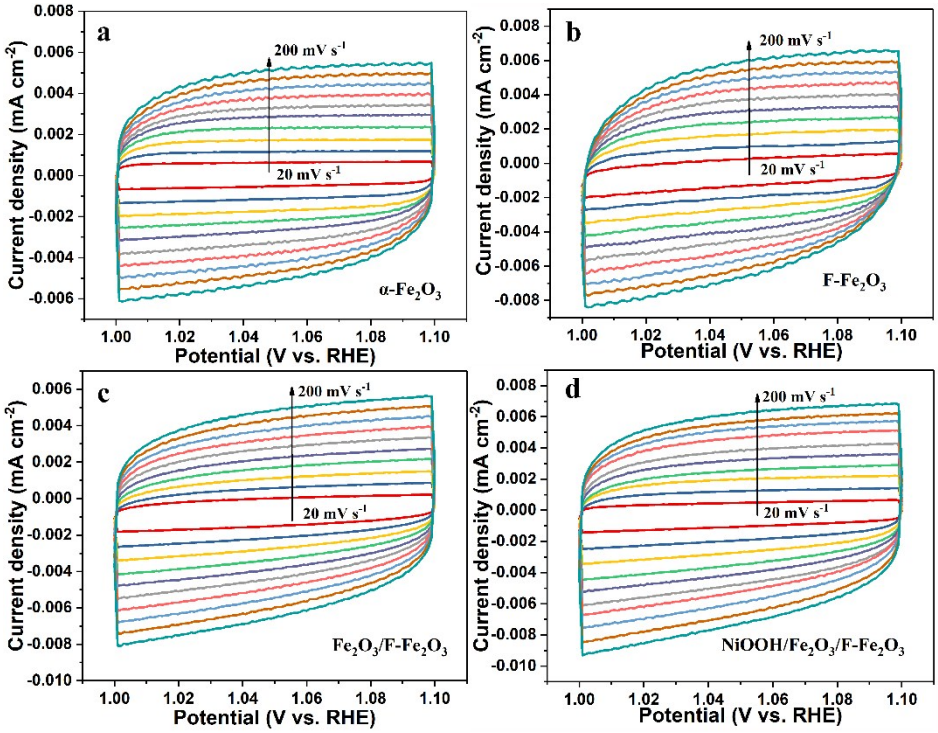

Figure S9. Voltammograms of the(a) α-Fe_2O_3, (b) F-Fe_2O_3, (c) Fe_2O_3/F-Fe_2O_3, and (d) NiOOH-Fe_2O_3/F-Fe_2O_3 NRs photoanodes at various scan rates (20-180 mV s^{-1})

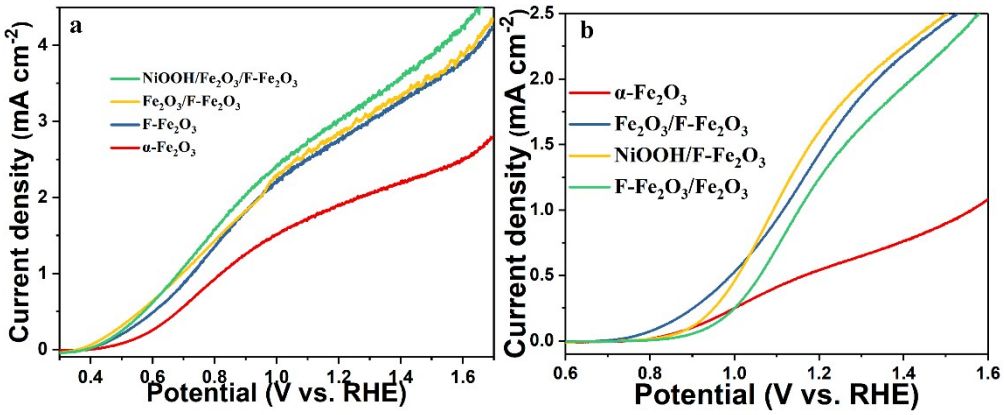

Figure S10. (a) LSVs of each photoanode collected at 5 mV s^{-1} in a 1 M Na_2SO_3 aqueous electrolyte under one sun illumination (100 mW cm^{-2}) and (b) photocurrent density vs. applied potential curves for each sample.

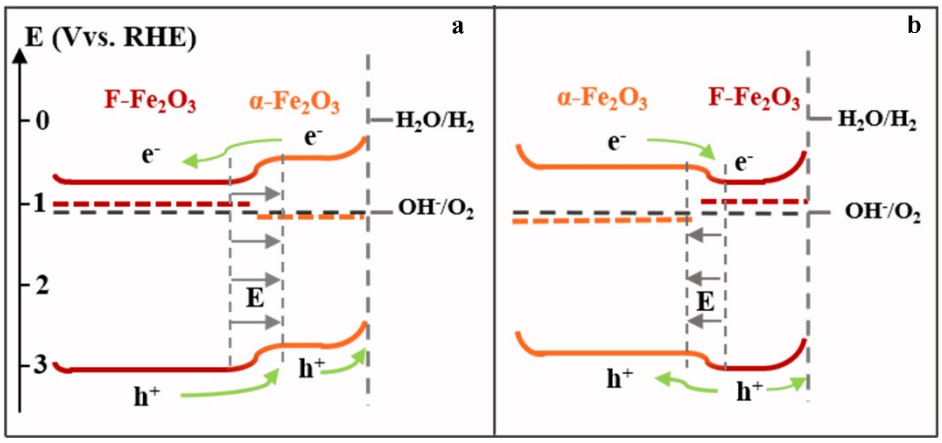

Figure S11. Energy band diagrams of (a) Fe_2O_3/F-Fe_2O_3 NRs and (b) F-Fe_2O_3/Fe_2O_3 NRs in solution.

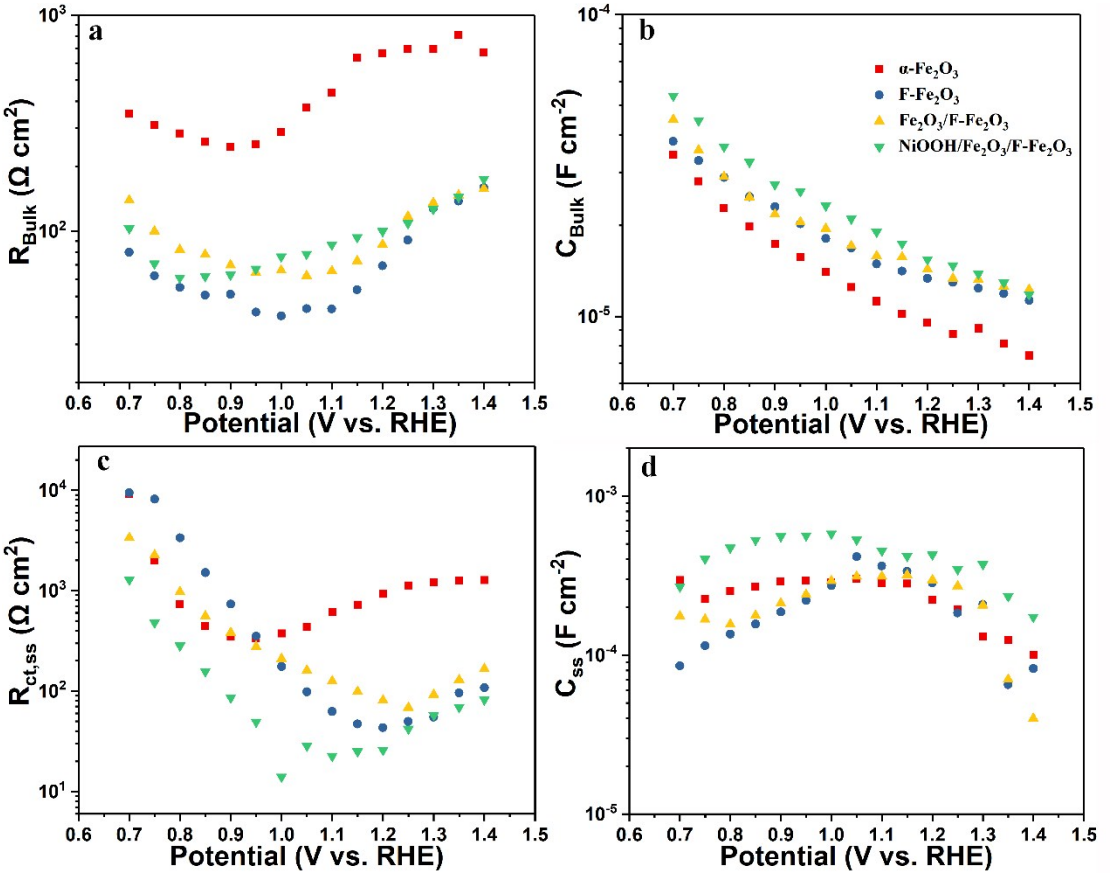

Figure S12. (a) R_{Bulk}, (b) C_{Bulk} (c) $R_{ct,\ ss}$ and (d) C_{ss} based on the equivalent circuit at different potentials of the each photoanode.

Table S1 Comparison of our photoanode to other α-Fe_2O_3-based photoanode

Catalyst	The onset potential (V vs.RHE)	Current density at 1.23 V vs. RHE (mA cm^{-2})	IPCE value (%)	Ref.
NiOOH/ Fe_2O_3/ F-Fe_2O_3	0.61	2.48	51 at 1.23V (300 nm)	THIS WORK
Fe_2O_3-TiO_2-40,	1.0	~ 0.2	14 at 1.23V (375 nm)	*Angew. Chem. Int. Ed*. **2018**, DOI: 10.1002/anie.201808104
Fh/Ti-Fe_2O_3	0.93	2.32	45 at 1.23V (320 nm)	*ChemSusChem* **2018**, DOI: 10.1002/cssc.201801406
FeFx-Fe_2O_3-Pt	~ 0.61	2.4	40 at 1.23V (350 nm)	*J. Mater. Chem. A,* **2018**, DOI: 10.1039/C8TA07622G
Dual axial gradient-codoped (Zr and Sn) Fe_2O_3 nanorod	~ 0.63	1.64	34 at 1.23V (410 nm)	*ChemSusChem* **2018,** DOI: 10.1002/cssc.201801614
Fe_2O_3/ F:FeOOH/ FeNiOOH	0.45	1.5	no	*ChemSusChem* **2018** DOI: 10.1002/cssc.201801751
Mg-Fe_2O_3/P-Fe_2O_3	0.68	2.4	36 at 1.23V (300 nm)	*J. Mater. Chem. A*, **2018**, 6, 13412
NiO/P-a-Fe_2O_3	0.69	2.08	38.6 at 1.23V (350 nm)	*ChemSusChem* **2018**, 11, 2156 – 2164
Fe_2O_3/Reassembled Carbon Nitride/CoPi	~0.65	0.7	32 at 1.23V (380 nm)	*ACS Appl. Mater. Interfaces,* **2018**, 10, 6424−6432
$CoFeO_x$ on hematite	0.6	1.2	~20 at 1.23V (360 nm)	*Energy Environ. Sci.,* **2018**, DOI: 10.1039/C8EE01346B
$Fe_{1-x}Ni_xOOH$	0.82	0.5	no	*ACS Catal.* **2018**,

on α-Fe_2O_3				8, 2754−2759
Sn-doped dodecahedral α-Fe_2O_3 on NFs/NiOOH	0.8	2.9	68 at 1.5V (360 nm)	*Nano Energy* **2018**, 50, 331–338
MnO_2/P:Fe_2O_3	~ 0.8	1.65	11.42 at 1.23V (350 nm)	*J. Mater. Chem. A,* **2018**, 6, 7021-7026
Sn-D-NFs/FeOOH	0.75	2.4	66 at 1.23V (350 nm)	*Nano Energy* **2018**, 50, 331-338.
grad-P:Fe_2O_3/Co-Pi	0.8	2.0	28 at 1.23V (300 nm)	*Chem. Sci*., **2017**, 8, 91–100
Zr-Fe_2O_3 NT	~ 0.89	1.50	25.7 at 1.23V (370 nm)	*Angew. Chem. Int. Ed*. **2017**, 129, 1 – 7
Rh−F-Fe_2TiO_5/Fe_2O_3	0.63	2.12	37 at 1.25V (370 nm)	*ACS Catal.* **2017**, 7, 4062−4069
C coated Fe_2O_3	0.77	2.0	no	*Appl. Catal. B-Environ.*, **2017**, 207, 1–8
C/Co_3O_4–Fe_2O_3	0.77	1.48	28 at 1.23V (325 nm)	*Angew. Chem. Int. Ed.***2016**, 55, 5851-5855
Co-Pi-Fe_2O_3	~ 0.8	1.28	no	*J. Catal.*, **2017**, 350, 48–55
IrO_2/RuO_2-Fe_2O_3	0.48	1.52	54 at at 1.25V (330 nm)	*Nano Energy* **2017**, 38, 218–231
E−I−Sn−Fe_2O_3	~ 0.6	2.2	27 at 1.23V (330 nm)	*Nano Lett.*, **2017**, 17, 2490–2495
Au-embedded α-Fe_2O_3	0.8	1.025	16 at 1.23V (410 nm)	*Chem.Commun.*, **2017**,53, 4278-4281
CoPi/TiO_2/Fe_2O_3	0.55	~ 6.0	56 at 1.23V (300 nm)	*Nano Energy* **2017**, 39, 211–218
FeOOH/Fe_2O_3	0.65	1.21	no	*Angew. Chem. Int. Ed*. **2016**, 55, 10854

Ru–Fe_2O_3	0.71	5.7	82 at 1.23V (320 nm)	Nano Energy **2015**, 16, 320–328
Mg-Fe_2O_3/ Fe_2O_3 film	0.8	~ 0.5	19 at 1.0 V (300 nm)	*J. Am. Chem. Soc*. **2012**, 134, 5508−5511

Reference

[1] J. Li, S. K. Cushing, P. Zheng, T. Senty, F. Meng, A. D. Bristow, A. Manivannan, N. Wu, *J. Am. Chem. Soc.,* **2014**, *136*, 8438-8449.

[2] F. Wang, W. Septina, A. Chemseddine, F. F. Abdi, D. Friedrich, P. Bogdanoff, R. van de Krol, S. D. Tilley, S. P. Berglund, *J. Am. Chem. Soc.,* **2017**. 139, 42, 15094-15103.

[3] C. Li, A. Li, Z. Luo, J. Zhang, X. Chang, Z. Huang, T. Wang, J. Gong, *Angew. Chem. Int. Ed.* **2017**, *129*, 4214-4219.

[4] W. Bian, Y. Huang, X. Xu, M. A. Ud Din, G. Xie, X. Wang, *ACS Appl. Mater. Interfaces,* **2018**, *10*, 9407-9414.